Theor Chem Acc (2009) 124:85–93
DOI 10.1007/s00214-009-0585-1

REGULAR ARTICLE

A CASSCF/CASPT2 study on the low-lying excited states of HSiCN, HSiNC and their ions

Zeng-Xia Zhao · Chun-Yuan Hou · Xin Shu · Hong-Xing Zhang · Chia-chung Sun

Received: 14 January 2009 / Accepted: 8 May 2009 / Published online: 24 May 2009

Abstract Equilibrium geometries of low-lying electronic states of cyanosilylene (HSiCN), isocyanosilylene (HSiNC), and their ions have been investigated using the complete active space self-consistent field (CASSCF) approach. The harmonic vibrational frequencies on the optimized geometries were calculated using the multiconfiguration linear response (MCLR) method. Taking the further correlation effects into account, the complete active space perturbation theory of second-order (CASPT2) was carried out for the energetic correction. The CASPT2 calculations have been performed to obtain the vertical excitation energies of selected low-lying excited states of HSiCN and HSiNC. Computed results show that the singlet-triplet splittings are calculated to be 0.99 and 1.30 eV for HSiCN and HSiNC, respectively. The vertical excitation energies of the lowest singlet and triplet excited states in HSiCN are lower than those in HSiNC. The first vertical ionization energy of HSiCN (10.04 eV) is higher than that of HSiNC (9.97 eV). The ground-state adiabatic electron affinities are found to be rather high, and the value of HSiCN (1.85 eV) higher than that of HSiNC (1.52 eV). The existences of dipole-bound excited negative ion states have been discovered within HSiCN and HSiNC.

Keywords CASSCF · CASPT2 · Excited state · Vertical transition energy

Z.-X. Zhao · C.-Y. Hou · X. Shu · H.-X. Zhang (✉) · C. Sun
Institute of Theoretical Chemistry, State Key Laboratory of Theoretical and Computational Chemistry, Jilin University, 130023 Changchun, People's Republic of China
e-mail: zhanghx@jlu.edu.cn

1 Introduction

The cosmic abundance of silicon is thought to be only slightly lower than those of C, N, and O [1], a surprisingly rich silicon chemistry has been discovered, even in regions where the temperature is fairly low. Of the 130 or so gas-phase astronomical molecules, approximately 10 silicon containing species have been detected in space, including SiO, SiC, SiC_2, cyclic-SiC_3, SiCN and SiNC et al. [2–5], and it is likely that with better spectroscopic data from the laboratory, many more may be found. The intensive search [6–15] for silicon-containing molecules of astrophysical interest has in the fact led to the discovery of HSiCN and HSiNC in discharge experiments in the laboratory by Sanz et al. [16]. Both of these species were regarded as being very strong candidates for detection in the interstellar medium, because similar species had already been observed in space (e.g. SiCN). Sanz et al. also found that both HSiCN and HSiNC have C_s symmetry with the H–Si–X (X = C or N) angle being $\sim 95°$. Dover and Evans have recently carried out laser-induced fluorescence spectroscopy on the $^1A''$ electronic state of HSiNC and found that upon excitation the H–Si–N angle increased by $\sim 20°$ [17].

The theoretical studies on cyanosilylene focused on the problem of the ground-state equilibrium structure of the HSiCN molecule, and those on HSiNC are rather sparse. The singlet-triplet splitting of the HSiCN was investigated by Kalcher [18]. Kalcher also predicted that all excited $HSiCN^-$ negative ion states can be characterized as dipole-bound states. Wang et al. [6] performed a detailed theoretical study on the neutral, cationic and anionic [H, Si, C, N] PES.

It is noteworthy that all the previous theoretical and experimental studies were concerned with only the ground state $^1A'$ and triplet state $^3A''$of HSiCN and HSiNC. So far, there has been no extensive work addressing their more

excited states, experimentally or theoretically. In an effort to understand more about these molecules, which are of potential importance in astrophysical chemistry, we carried out a study on the excited states of HSiCN, HSiNC and also their ionic states using high level ab initio molecular orbital theory (CASSCF/CASPT2) [19–23], which have proved to be effective for theoretical studies of electronic excited states of molecules. Therefore, in this study, the equilibrium geometries, harmonic frequencies, the energies of the ground state and the partial excited states for HSiCN and HSiNC have been investigated. This article reports, for the first time, the vertical transition energies of HSiCN and HSiNC.

1.1 Computational methods

The geometries and the atom labelings used for HSiCN and HSiNC (C_s symmetry) are shown in Fig. 1. Choice of the active space is the essential step in the calculations with the CASSCF/CASPT2 method. The wave function includes all excitations of 14 valence electrons in 13 molecular orbitals, corresponding to the valence atomic s, p orbitals of C, N, and Si atoms and 1s orbital of the H atom, namely, ten a' orbitals and three a'' orbitals.

The geometry of every state was optimized at the CASSCF [24] level of theory. Multiconfigurational linear response (MCLR) [25] -computed response calculations on single multiconfigurational SCF wave functions, which was used to compute the harmonic frequency, and complete active space second-order perturbation (CASPT2) [26] was used to calculate the dynamic correction. The calculations were performed using the augmented correlation consistent valence triple-zeta aug-cc-pVTZ basis set [27, 28]. According to the CASPT2 energies calculated at the corresponding geometries optimized at the CASSCF level, we obtained the CASSCF/CASPT2 adiabatic excitation energy values of the selected excited states, denoted as T_a. Based on the CASPT2 energy calculations at the CASSCF geometries of the ground state for HSiCN and HSiNC, we obtained the CASSCF/CASPT2 vertical excitation energies for the 11 excited states, denoted as T_v.

The oscillator strength is defined as $f = 2(\mathrm{TDM})^2\Delta E/3$. The transition moments (TDM) were computed by CASSCF, and the excitation energies, which are very sensitive to dynamic correlation, were computed by CASPT2.

The optimized geometries of the ground state for HSiCN and HSiNC were used to calculate the vertical ionization potentials (VIP). The calculated adiabatic ionization energies (AIP) are obtained from the difference of the total energies between the radical ion and the neutral HSiCN and HSiNC radical in their optimized geometries, respectively. All the CAS calculations were performed using the MOLCAS 6.2 quantum-chemistry software [29].

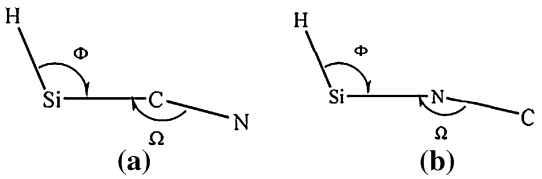

Fig. 1 Sketch of the molecular geometries of **a** HSiCN and **b** HSiNC

2 Results and discussion

2.1 HSiCN and HSiNC

2.1.1 *Equilibrium geometries of the ground state and excited states of HSiCN and HSiNC*

It is instructive to consider first the parent species: SiH_2. The SiH_2 molecule has been the subject of considerable experimental and theoretical interest [30–34]. A comparison of the results of these high-level studies should provide a realistic assessment of the accuracy for the theoretical methods applied in this work for HSiCN and HSiNC. The ground electronic state of SiH_2 is a singlet $^1A_1$ state (in the C_{2v} symmetry point group). In this work, the equilibrium molecular parameters for the $^1A_1$ and $^3B_1$ states of SiH_2 were calculated at the CASSCF(6,6)/aug-cc-pVTZ/CASPT2(6,6)/aug-cc-pVTZ level of theoretical studies. The singlet–triplet energy difference was calculated to be 0.75 eV. The estimated values can be compared with those calculated at various levels of theory [31–34] and experimental results [30]. Turning to the main subject of this study, Tables 1, 2, 3, 4, 5, 6, 7, and 8 list the relative information of the low-lying electronic states of HSiCN, HSiNC and also their ions. To explain the differences in geometry among the ground and excited states, we presented, in Fig. 2, the plots of a part of orbitals of the active space which would be used in the following discussion. Using these data, the singlet–triplet energy differences for HSiCN (0.99 eV) and HSiNC (1.30 eV) are predicted to be slightly higher than that for the parent SiH_2 molecule. As shown in Table 3 and Fig. 2, the conjugation between the Si and N atom in HSiCN and HSiNC lower both the energies of HOMO and LUMO orbitals of SiH_2. The calculated energies of HOMO–LUMO energy gaps ΔE follow this order: $\Delta E(\mathrm{HSiNC}) > \Delta E(\mathrm{HSiCN}) > \Delta E(\mathrm{SiH_2})$. Thus, the singlet–triplet splittings of HSiCN and HSiNC are larger than that of SiH_2, and the singlet–triplet splitting of HSiNC is larger than that of HSiCN.

Table 1 lists key geometrical parameters of the five low-lying states for the HSiCN and HSiNC, respectively, which

Table 1 Optimization structures, leading configurations occupation, and respective weights in the CI vector (c^2), adiabatic excitation energies (T_a in eV), and dipole moment for the low-lying electronic states of HSiCN and HSiNC at C_s symmetry at the CASSCF/CASPT2 level of theory using aug-cc-pVTZ basis sets

Species	State	R_{HSi} (Å)	R_{SiX}(Å) (X=C or N)	R_{CN} (Å)	Ω (°)	Φ (°)	Configurations		T_a' (CASSCF) (in eV)	T_a (CASPT2) (in eV)	Dipole moment (in Debye)
							Weight	Occupation[a]			
HSiCN	X^1A'	1.534	1.887	1.169	175.5	94.3	0.867	$(9a')^2(10a')^2(11a')^2(2a'')^2(12a')^2(3a'')^0$	0.00	0.00	3.3
	[b]	1.524	1.886	1.169	174.2	92.0					
	[c]	1.515	1.886	1.166	174.2	92.2					
	$^3A''$	1.469	1.854	1.169	177.9	116.1	0.906	$(9a')^2(10a')^2(11a')^2(2a'')^2(12a')^\alpha(3a'')^\alpha$	0.93	0.99	3.6
	[b]	1.488	1.811	1.172	176.6	116.8					
	[c]	1.478	1.827	1.166	177.1	116.7					
	$^1A''$	1.520	1.842	1.176	177.8	119.5	0.876	$(9a')^2(10a')^2(11a')^2(2a'')^2(12a')^\alpha(3a'')^\beta$	2.25	1.97	3.4
	$2^3A''$	1.717	1.864	1.176	174.5	64.9	0.833	$(9a')^2(10a')^\alpha(11a')^2(2a'')^2(12a')^2(3a'')^\alpha$	4.14	3.56	3.2
	$^3A'$	1.511	1.902	1.275	172.0	89.9	0.881	$(9a')^2(10a')^2(11a')^2(2a'')^\alpha(12a')^2(3a'')^\alpha$	4.65	4.28	0.5
HSiNC	X^1A'	1.536	1.788	1.187	172.9	95.5	0.882	$(9a')^2(10a')^2(11a')^2(2a'')^2(12a')^2(3a'')^0$	0.00	0.00	3.2
	[b]	1.511	1.772	1.189	172.3	93.8					
	$^3A''$	1.468	1.757	1.184	176.3	114.3	0.916	$(9a')^2(10a')^2(11a')^2(2a'')^2(12a')^\alpha(3a'')^\alpha$	1.33	1.30	3.6
	[b]	1.493	1.727	1.193	174.9	114.6					
	$^1A''$	1.540	1.751	1.190	175.4	116.5	0.888	$(9a')^2(10a')^2(11a')^2(2a'')^2(12a')^\alpha(3a'')^\beta$	2.54	2.37	3.4
	$2^3A''$	1.552	1.920	1.179	166.2	85.2	0.927	$(9a')^2(10a')^2(11a')^\alpha(2a'')^2(12a')^2(3a'')^\alpha$	4.05	3.80	3.7
	$^3A'$	1.514	2.808	1.241	177.9	80.2	0.888	$(9a')^2(10a')^2(11a')^2(2a'')^\alpha(12a')^2(3a'')^\alpha$	5.36	5.70	0.8

[a] The occupation number represents the electronic number that is occupied in the active space. α represents a spin-up electron, β represents a spin-down electron, and 2 represents double occupied electrons. Every state has common configuration (core)$(7a')^2(8a')^2$, we will not present in the table

[b] Ref. [6]. Calculated at the B3LYP/6-31G(*d*) level

[c] Ref. [18]. Calculated at the ACPF/aug-cc-pVTZ level

Table 2 Vibration frequencies for the ground and excited states of HSiCN and HSiNC calculated by MCLR

Species	State	Harmonic vibration frequency (cm^{-1})					
		ω_1 (a')	ω_2 (a')	ω_3 (a')	ω_4 (a')	ω_5 (a')	ω_6 (a'')
HSiCN	X^1A'	2,197.5	2,016.7	827.8	572.6	271.1	232.2
	[a]Expt.	2,142.7	2,026.7	826.4	563.5		
	$^1A''$	2,107.9	1,947.5	661.6	588.9	252.7	322.0
	$^3A''$	2,193.7	2,165.0	702.5	626.5	263.4	313.0
	$2^3A''$	2,087.2	1,398.6	913.6	557.5	334.2	321.9
	$^3A'$	2,147.3	1,563.1	820.4	515.6	277.8	283.9
HSiNC	X^1A'	2,080.5	2,041.1	928.3	617.4	226.1	300.2
	[a]Expt.	2,039.5	2,017.8	867.9	622.0		
	$^1A''$	2,035.9	1,780.6	657.6	612.5	191.3	248.5
	$^3A''$	2,148.2	2,078.9	708.2	658.6	186.8	224.9
	$2^3A''$	1,965.3	1,862.3	770.5	333.2	277.5	304.2
	$^3A'$	2,137.0	1,803.2	458.4	83.7	63.7	109.6

For HSiCN, ω_1 represents the H–SiCN stretch, ω_2 represents the HSi–CN asym stretch, ω_3 represents the HSi–CN sym stretch, ω_4 represents the H–Si–CN out-phase bend, ω_5 H–Si–CN in-phase bend, and ω_6 represents the HSi–CN bend

For HSiNC, ω_1 represents the H–SiNC stretch, ω_2 represents the HSi–NC asym stretch, ω_3 represents the HSi–NC sym stretch, ω_4 represents the H–Si–NC out-phase bend, ω_5 H–Si–NC in-phase bend, and ω_6 represents the HSi–NC bend

[a] Ref. [35]

also contain adiabatic excitation energies, leading configurations, and dipole moments. Table 1 shows that the neutral HSiCN and HSiNC with closed-shell electronic configurations both have singlet ground states X^1A'. CASSCF wavefunction analysis shows that weight in CI vector (c^2) of ground state for HSiCN and HSiNC are 0.867 and 0.882, respectively. Such large weights indicate that the contributions of these configurations are dominant in their ground states. The equilibrium geometry parameters of ground states of X^1A' for the HSiCN and HSiNC we obtained accord with experimental and previous theoretical values.

We will briefly describe the CASSCF geometries of selected excited states in comparison with the geometry of the HSiCN and HSiNC, respectively, as follows. For HSiCN, the HOMO–LUMO single electron excitation $12a' \rightarrow 3a''$ leads to the two states $^1A''$ and $^3A''$ states, which can be described as single configuration (core)$(7a')^2(8a')^2(9a')^2(10a')^2(11a')^2(2a'')^2(12a')^\alpha(3a'')^\beta$ and (core)$(7a')^2$ $(8a')^2(9a')^2(10a')^2(2a'')^2(11a')^2(12a')^\alpha(3a'')^\alpha$ and with weights of 0.876 and 0.906, respectively. $12a'$ and $3a''$ show mainly dominant n(Si:$3sp_xp_y$) and n(Si:$3p_z$) non-bonding characters and relatively little π^*(Si–N) (Si–N antibonding) contributions from the N atom. The single electron transitions shorten the R_{HSi} and R_{SiC} bond lengths, and increase Φ bond angle.

Table 3 The orbital energies of HOMO and LUMO for SiH_2, HSiCN and HSiNC

Orbital energy (in Hartree)	SiH_2	HSiCN	HSiNC
HOMO	−0.3367	−0.3751	−0.3616
LUMO	−0.0035	−0.0301	−0.0116
HOMO–LUMO gap	0.3402	0.3450	0.3500

The $2^3A''$ can be seen as a single-electron transition configuration $10a' \rightarrow 3a''$ with a weight of 0.833. The elongating of the Si–H bond in $2^3A''$ can be understood by reducing the bonding interaction between the Si–H atoms in the $10a'$. As compared with the C–N bond length in the geometry of the ground state for HSiCN, the $^3A'$ has very long C–N bond length, because one electron promotes from the $2a''$ bonding orbital ($2a''$ is of π character coming from the interaction of the $2p_z$ of the C and N atoms) to the non-bonding $3a''$ orbital.

For HSiNC, the $^1A''$ and $^3A''$ states can be described as single transition configuration $12a' \rightarrow 3a''$ with weights of 0.888 and 0.916, respectively, but have different spins. $12a'$ has mainly of dominant $n(\text{Si:}3sp_xp_y)$ non-bonding character and relative little π^*(Si–N) contributions from the N atom. $3a''$ shows mainly dominant $n(\text{Si:}3p_z)$ non-bonding character. The single electron transitions shorten the R_{HSi} and R_{SiC} bond lengths, and increase Φ bond angle. As compared with the C–N bond lengths in the geometry of the ground state for HSiNC, the $^3A'$ has very long C–N bond length, because one electron promotes from the $2a''$ bonding orbital ($2a''$ is of π character coming from the interaction of the $2p_z$ of the C and N atoms) to the $3a''$ orbital. The $2^3A''$ state can be simply viewed as $11a' \rightarrow 3a''$ single electron transition, with a weight of 0.927. The $11a'$ orbital can be described as an N–H sigma orbital as seen in Fig 2a, while the $3a''$ presents $n(\text{Si:}3p_z)$ non-bonding. Thus, the single electron transition shortens the R_{CN}, elongates the R_{SiH} and R_{SiN}, decreases the bond angles Ω and Φ.

The frequency values of HSiCN and HSiNC are summarized in Table 2 at the CASSCF level using the MCLR method. Available experimental frequency values in the four modes of the ground state are listed in Table 2. As shown in Table 2, the CASSCF frequencies of HSiCN ω_1 (2,197.5 cm^{-1}, H–SiCN stretch), ω_2 (2,016.7 cm^{-1}, His–CN asymmetry stretch), ω_3 (827.8 cm^{-1}, H–SiCN symmetry stretch), and ω_4 (572.6 cm^{-1}, H–Si–CN out-plane bend) show good agreement with the experimental values, 2,142.7, 2,026.7, 826.4, and 563.5 cm^{-1}. The CASSCF harmonic frequencies of HSiNC also agree well with the experimental results, and the deviation is about 7% between the calculated and experimental data. The CASSCF frequency calculations produced no imaginary frequencies for the calculated electronic states of HSiCN and HSiNC.

Table 4 Vertical excitation energies (T_v) (in eV) and oscillator strengths (f) calculated at the CASSCF/CASPT2 level for HSiCN and HSiNC

HSiCN	State	Transition	T_v	f	HSiNC	State	Transition	T_v	f
	X^1A'		0.000	Ground state		X^1A'	0.000	Ground state	
	$^3A''$	$12a' \rightarrow 3a''$	1.15	$<10^{-10}$		$^3A''$	$12a' \rightarrow 3a''$	1.28	$<10^{-10}$
	$^1A''$	$12a' \rightarrow 3a''$	2.22	2.03×10^{-2}		$^1A''$	$12a' \rightarrow 3a''$	2.39	1.65×10^{-2}
	$^3A'$	$2a'' \rightarrow 3a''$	3.51	$<10^{-10}$		$2^3A''$	$10a' \rightarrow 3a''$ $11a' \rightarrow 3a''$	3.68	$<10^{-10}$
	$2^3A''$	$11a' \rightarrow 3a''$	4.47	$<10^{-10}$		$2^1A''$	$11a' \rightarrow 3a''$ $12a' \rightarrow 3a''$	4.33	6.83×10^{-3}
	$2^1A''$	$11a' \rightarrow 3a''$	4.79	4.74×10^{-3}		$3^3A''$	$10a' \rightarrow 3a''$ $11a' \rightarrow 3a''$ $12a' \rightarrow 3a''$	5.48	$<10^{-10}$
	$3^3A''$	$9a' \rightarrow 3a''$ $11a' \rightarrow 3a''$	5.09	$<10^{-10}$		$2^1A'$	$(12a')^2 \rightarrow (3a'')^2$ $11a'12a' \rightarrow (3a'')^2$	5.56	6.64×10^{-3}
	$2^1A'$	$(12a')^2 \rightarrow (3a'')^2$	5.36	1.68×10^{-2}		$^3A'$	$2a'' \rightarrow 3a''$	5.65	$<10^{-10}$
	$3^1A''$	$9a' \rightarrow 3a''$	5.45	2.32×10^{-4}		$2^3A'$	$2a'' \rightarrow 3a''$	5.78	$<10^{-10}$
	$3^1A'$	$2a'' \rightarrow 3a''$	5.62	5.79×10^{-2}		$3^1A'$	$(12a')^2 \rightarrow (3a'')^2$ $11a'12a' \rightarrow (3a'')^2$	5.86	$<10^{-10}$
	$2^3A'$	$9a' \rightarrow 13a'$ $12a' \rightarrow 13a'$	6.64	$<10^{-10}$		$3^1A''$	$10a' \rightarrow 3a''$ $11a' \rightarrow 3a''$ $12a' \rightarrow 3a''$	5.92	8.68×10^{-3}
	$3^3A'$	$12a' \rightarrow 3a''$	7.08	$<10^{-10}$		$3^3A'$	$12a' \rightarrow 3a''$	5.98	$<10^{-10}$

Table 5 Optimization structures, leading configurations occupation, and respective weights in the CI vector (c^2), adiabatic excitation energies (T_a in eV), and dipole moment for the low-lying electronic states of $HSiCN^+$ and $HSiNC^+$ at C_s symmetry at the CASSCF/CASPT2 level of theory using aug-cc-pVTZ basis sets

Species	State	R_{SiH} (Å)	R_{SiX} (Å) (X=C or N)	R_{CN} (Å)	Ω (°)	Φ (°)	Configurations		Ta (CASSCF) (eV)	Ta (CASPT2) (eV)	Dipole moment (in Debye)
							Weight	Occupation[a]			
$HSiCN^+$	X^2A'	1.500	1.803	1.178	175.6	118.7	0.883	$(9a')^2(10a')^2(11a')^2(2a'')^2(12a')^\alpha(3a'')^0(13a')^0$	0.00	0.00	5.4
	[b]	1.496	1.790	1.173	176.5	116.5					
	$^2A''$	1.495	2.202	1.229	175.9	86.3	0.875	$(9a')^2(10a')^2(11a')^2(2a'')^\alpha(12a')^2(3a'')^0(13a')^0$	2.38	2.78	1.8
	$^4A'$	1.494	1.894	1.250	176.8	112.5	0.891	$(9a')^2(10a')^2(11a')^2(2a'')^\alpha(12a')^\alpha(3a'')^\alpha(13a')^0$	3.47	3.52	1.5
	$^4A''$	1.498	1.920	1.205	158.9	107.9	0.874	$(9a')^2(10a')^2(11a')^2(2a'')^2(12a')^\alpha(3a'')^\alpha(13a')^\alpha$	3.50	3.59	0.6
$HSiNC^+$	X^2A'	1.513	1.669	1.212	171.4	117.4	0.903	$(9a')^2(10a')^2(11a')^2(2a'')^2(12a')^\alpha(3a'')^0(13a')^0$	0.00	0.00	4.6
	[b]	1.505	1.670	1.211	174.7	114.5					
	$^4A''$	1.492	1.842	1.163	174.4	108.5	0.863	$(9a')^2(10a')^2(11a')^2(2a'')^\alpha(12a')^\alpha(3a'')^\alpha(13a')^0$	2.35	2.69	1.7
	$^2A''$	1.491	2.222	1.254	174.9	85.6	0.876	$(9a')^2(10a')^2(11a')^2(2a'')^\alpha(12a')^2(3a'')^0(13a')^0$	2.94	3.24	2.6
	$^4A'$	1.495	1.983	1.258	178.4	106.7	0.900	$(9a')^2(10a')^2(11a')^2(2a'')^2(12a')^\alpha(3a'')^\alpha(13a')^\alpha$	4.43	4.73	1.0

[a] The occupation number represents the electronic number that is occupied in the active space. α represents a spin-up electron, β represents a spin-down electron, and 2 represents double occupied electrons. Every state has common configuration (core)$(7a')^2(8a')^2$, we will not present in the table

[b] Ref. [6]. Calculated at the B3LYP/6-31G(*d*) level

Table 6 The calculated vertical and adiabatic IPs (in eV) of HSiCN and HSiNC

Species	State	Adiabatic IPs	Vertical IPs	Species	State	Adiabatic IPs	Vertical IPs
HSiCN	X^2A'	9.67	10.04	HSiNC	X^2A'	9.43	9.97
	$^2A''$	12.45	12.82		$^2A''$	12.67	10.79
	$^4A'$	13.19	13.62		$^4A'$	12.12	12.19
	$^4A''$	13.26	13.36		$^4A''$	14.16	14.55

2.1.2 Vertical excitation energies

Vertical excitation energies are very helpful in explaining spectral features due to the Franck–Condon principle. To date, the study of the photoinduced absorption for HSiCN and HSiNC has not been addressed either experimentally or theoretically. Little is known about the nature of their excited states. In the present work, we have calculated the vertical excitation energies for the following excited states of HSiCN and HSiNC, respectively, $2^1A'$, $3^1A'$, $^1A''$, $2^1A''$, $3^1A''$, $^3A''$, $2^3A''$, $3^3A''$, $^3A'$, $2^3A'$, and $3^3A'$ at the CASSCF/CASPT2/aug-cc-pVTZ level. The results for the vertical excitation energies are listed in Table 4. Among these electronic excitations, the $X^1A' \rightarrow {}^1A'$ and $X^1A' \rightarrow {}^1A''$ are allowed by the spin and dipole rules.

For HSiCN besides the HOMO–LUMO excitation also transitions from the HOMO into other virtual orbital ($13a'$) and transitions from the other occupied ($9a'$, $10a'$, $11a'$, $2a''$) orbitals into LUMO are found to play an important role in the electronic spectrum. In the CASPT2 calculations, among the allowed transitions the energy of $X^1A' \rightarrow {}^1A''$ is the lowest. We assigned it to be $n_{xy}(a') \rightarrow n_z(a'')$ in nature, which is 2.218 eV with an oscillator strength (*f*) of 2.03×10^{-2}, whereas $X^1A' \rightarrow 3^1A'$ transition is the most intense transition with a vertical transition energy 5.62 eV and an oscillator strength (*f*) of 5.79×10^{-2}, which is assigned to be $\pi(a'') \rightarrow n_z(a'')$ in nature.

For HSiNC, besides the HOMO–LUMO excitation also transitions from the other occupied orbitals ($9a'$, $10a'$, $11a'$, $2a''$) into LUMO are found to play an important role in the electronic spectrum. In the CASPT2 calculations, among the allowed transitions the energy of $X^1A' \rightarrow {}^1A''$ is the lowest and most intensive transition. We assigned it to be $\pi(a'') \rightarrow n_z(a'')$ in nature, which is 2.39 eV with an oscillator strength (*f*) of 1.65×10^{-2}.

2.2 $HSiCN^+$ and $HSiNC^+$

2.2.1 Equilibrium geometries of the ground state and low-lying excited states for $HSiCN^+$ and $HSiNC^+$

Although there no experimental data available for the structure of the $HSiCN^+$ and $HSiNC^+$ cations, we here

Table 7 Optimization structures, leading configurations occupation, and respective weights in the CI vector (c^2), adiabatic excitation energies (T_a in eV), and dipole moment for the low-lying electronic states of $HSiCN^-$ and $HSiNC^-$ at C_s symmetry at the CASSCF/CASPT2 level of theory using aug-cc-pVTZ basis sets

Species	State	R_{SiH} (Å)	R_{SiX}(Å)$_{(X=C\ or\ N)}$	R_{CN} (Å)	Ω (°)	Φ (°)	Configuration		T_a' (CASSCF) (eV)	T_a (CASPT2) (eV)	Dipole moment (Debye)
							Weight	Occupation[a]			
$HSiCN^-$	X^2A''	1.561	1.958	1.178	175.2	92.9	0.901	$(9a')^2(10a')^2(11a')^2(2a'')^2(12a')^2(3a'')^\alpha(13a')^0(4a'')^0$	0.00	0.00	0.8
	[b]	1.549	1.910	1.176	174.5	92.1					
	[c]	1.537	1.928	1.172	174.7	91.7					
	$^2A'$	1.494	1.927	1.169	174.1	94.2	0.877	$(9a')^2(10a')^2(11a')^2(2a'')^2(12a')^2(3a'')^0(13a')^\alpha(4a'')^0$	1.75	2.52	11.5
	$^4A''$	1.466	1.859	1.169	179.1	114.3	0.921	$(9a')^2(10a')^2(11a')^2(2a'')^2(12a')^\alpha(3a'')^\alpha(13a')^\alpha(4a'')^0$	2.73	3.41	10.8
	$^4A'$	1.492	1.815	1.155	178.8	116.2	0.942	$(9a')^2(10a')^2(11a')^2(2a'')^2(12a')^\alpha(3a'')^\alpha(13a')^0(4a'')^\alpha$	4.88	4.22	5.3
$HSiNC^-$	X^2A''	1.561	1.901	1.182	175.0	92.7	0.912	$(9a')^2(10a')^2(11a')^2(2a'')^2(12a')^2(3a'')^\alpha(13a')^0(4a'')^0$	0.00	0.00	0.5
	[b]	1.553	1.854	1.184	172.4	92.9					
	$^2A'$	1.493	1.836	1.184	171.7	94.7	0.885	$(9a')^2(10a')^2(11a')^2(2a'')^2(12a')^2(3a'')^0(13a')^\alpha(4a'')^0$	1.64	2.25	11.5
	$^4A''$	1.462	1.179	1.184	175.5	112.8	0.929	$(9a')^2(10a')^2(11a')^2(2a'')^2(12a')^\alpha(3a'')^\alpha(13a')^\alpha(4a'')^0$	2.87	3.40	11.5
	$^4A'$	1.468	1.740	1.173	177.9	114.3	0.955	$(9a')^2(10a')^2(11a')^2(2a'')^2(12a')^\alpha(3a'')^\alpha(13a')^0(4a'')^\alpha$	4.92	4.25	0.7

[a] The occupation number represents the electronic number that is occupied in the active space. α represents a spin-up electron, β represents a spin-down electron, and 2 represents double occupied electrons. Every state has common configuration (core)$(7a')^2(8a')^2$, we will not present in the table

[b] Ref. [6]. Calculated at the B3LYP/6-31G(*d*) level

[c] Ref. [18]. Calculated at the ACPF/aug-cc-pVTZ level

Table 8 The Mulliken population analysis of $HSiCN^-$ and $HSiNC^-$

Atom	Orbital	State of $HSiCN^-$				State of $HSiNC^-$			
		X^2A''	$^2A'$	$^4A''$	$^4A'$	X^2A''	$^2A'$	$^4A''$	$^4A'$
N	*s*	3.8049	3.5911	3.6262	3.8125	3.3369	3.2454	3.2046	3.1942
	p_x	1.1679	1.1674	1.1177	1.0988	1.2818	1.2939	1.3469	1.3351
	p_y	1.2069	1.1848	1.1768	1.2102	0.9469	1.1963	1.1870	0.8509
	p_z	1.1564	1.0918	1.1458	1.3880	1.3081	1.3622	1.3174	0.5438
	Total	7.4047	7.1189	7.1492	7.5798	6.9263	7.1582	7.1476	5.9718
C	*s*	3.3036	4.1734	4.0315	3.2282	4.2038	4.5335	4.5266	4.2394
	p_x	0.7814	0.7699	0.8205	0.8364	0.6705	0.6547	0.5892	0.5920
	p_y	0.8945	0.9191	0.9233	0.8951	1.0589	1.1379	1.1214	1.0548
	p_z	0.8083	0.8438	0.8047	−0.0675	0.6570	0.5667	0.6216	1.1618
	Total	5.8607	6.7420	6.6588	4.9897	6.6506	6.9704	6.9389	7.1070
Si	*s*	5.7030	3.2842	2.8897	5.2134	5.5849	2.9320	2.5517	5.0959
	p_x	3.0113	2.8152	2.6555	2.6778	3.0239	2.8372	2.6208	2.6855
	p_y	2.7502	3.3930	3.1307	2.7013	2.5338	3.2710	3.0448	2.6043
	p_z	2.9706	2.1038	2.9408	4.6565	2.9887	2.1166	2.9659	4.2402
	Total	14.6229	11.8333	11.8061	15.3617	14.3056	11.3897	11.3683	14.8572
H	*s*	1.0834	3.3705	3.4281	1.0477	1.0894	3.5571	3.5885	1.0405
	Total	1.1118	3.3058	3.3859	1.0688	1.1175	3.4817	3.5451	1.0640

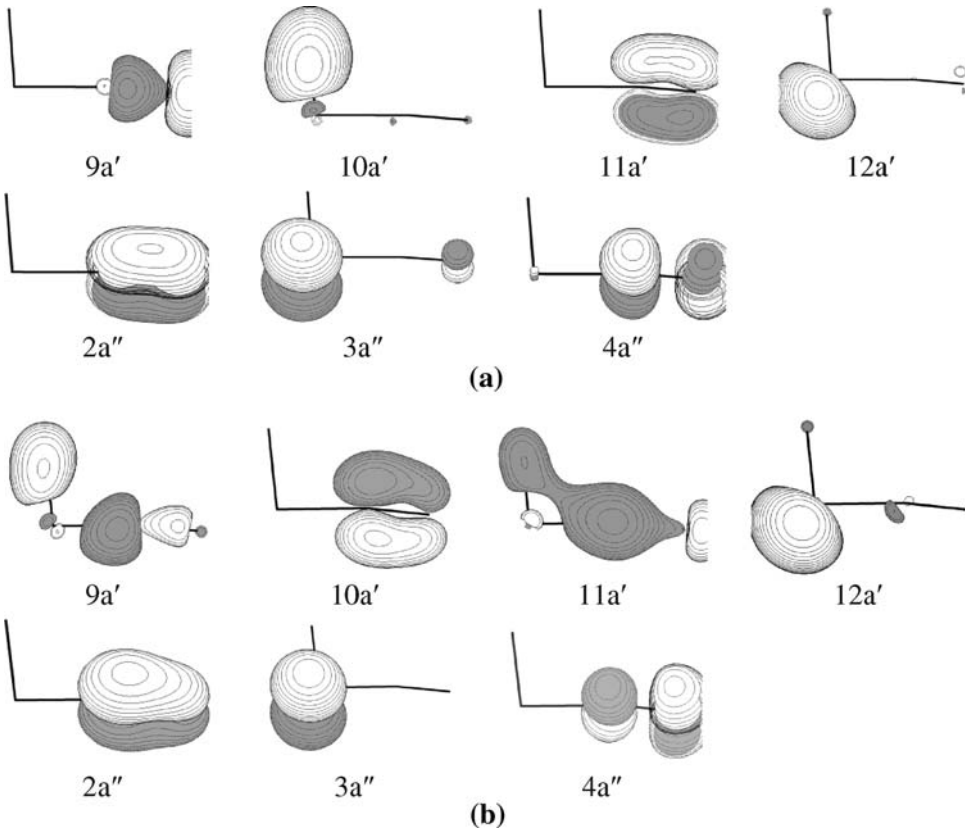

Fig. 2 The plots of a part of **a** HSiCN and **b** HSiNC orbitals in the active space

discuss their geometric structures for the both the ground and excited states, because $HSiCN^+$ and $HSiNC^+$ are the products from the photoelectron ionization of the HSiCN and HSiNC radicals, respectively. All the states for the C_s equilibrium geometry that we obtained at the CASSCF/CASPT2 level are summarized in Table 5. As shown in

Table 5, the X^2A' is predicted to be both the ground state of $HSiCN^+$ and $HSiNC^+$ cations, respectively. As compared to the ground state of neutral radical, the X^2A' of $HSiCN^+$ can result from removing an electron from the double occupied $12a'$ orbital of the X^1A' state of HSiCN. This electron's removal makes the R_{SiC} shorten to 0.110 Å and Φ is increased to 24.8°, but other geometry parameters are unchanged. The final structural parameters of $R_{HSi} = 1.500$ Å, $R_{SiC} = 1.803$ Å, $R_{CN} = 1.177$ Å, $\Omega = 175.3°$ and $\Phi = 118.7°$, consistent with the $R_{HSi} = 1.496$ Å, $R_{SiC} = 1.790$ Å, $R_{CN} = 1.172$ Å, $\Omega = 176.5°$ and $\Phi = 116.5°$ calculated by Wang et al. at the B3LYP/6-31G(*d*) level. Removing an electron from the double occupied $12a'$ orbital of the X^1A' state of HSiNC results in the X^2A' electronic ground state of $HSiNC^+$. As the $12a'$ is of small degree Si–N anti-bonding character, the Si–N bond length is shortened in the $HSiNC^+$ cation compared with the HSiNC molecule in the ground state. Our calculation results accord with the previous calculations.

The three low-lying excited states $^2A''$, $^4A''$ and $^4A'$ of $HSiCN^+$ and $HSiNC^+$ have a leading configuration whose weight above 0.800, indicating a single-reference character. As mentioned above, their geometrical structures alteration can be reasonably explained according to the electronic configuration (Table 5) and molecule orbitals (Fig. 2), and we do not discuss these results in detail there.

2.2.2 *Ionization potentials (IPs) of the HSiCN and HSiNC neutral radical*

There have been scarcely any photoelectron spectrum experimental and calculation reports about HSiCN and HSiNC. The adiabatic and vertical IPs (ionization potentials) of HSiCN and HSiNC we calculated are summarized in Table 6. As shown in Table 6, the first adiabatic IP of HSiCN and HSiNC are 9.67 and 9.43 eV, and the first vertical IP of HSiCN and HSiNC are 10.04 and 9.97 eV, respectively. The differences between the vertical and adiabatic ionization energies of HSiCN and HSiNC are 0.38 and 0.27 eV, respectively. This means that the HOMO ($12a'$) of the HSiCN and HSiNC are not absolutely non-bonding orbitals but with a small degree of Si–N interaction character.

2.3 $HSiCN^-$ and $HSiNC^-$

2.3.1 *Equilibrium geometries of the ground state and low-lying excited states of $HSiCN^-$ and $HSiNC^-$ anions*

The optimized geometrical structures for $HSiCN^-$ and $HSiNC^-$ were listed in Table 7. On the basis of adiabatic energies, the X^2A'' state is confirmed as the ground state of both $HSiCN^-$ and $HSiNC^-$ anions, respectively. As compared to the neutral radical's ground state, the X^2A'' state of HSiCN is mainly created by adding an electron to the unoccupied $3a''$ orbital of the X^1A' state of HSiCN. This electron's addition makes all bonding lengths are elongated, but bonding angles are almost unchanged. The geometrical parameters of the $^2A''$ state are $R_{HSi} = 1.561$ Å, $R_{SiC} = 1.958$ Å, $R_{CN} = 1.178$ Å, $\Omega = 175.2°$ and $\Phi = 92.9°$. The X^2A'' state of HSiNC is resulted from by adding an electron to the unoccupied $3a''$ orbital of the X^1A' state of HSiNC. The geometry our calculated are $R_{HSi} = 1.561$ Å, $R_{SiC} = 1.901$ Å, $R_{CN} = 1.182$ Å, $\Omega = 175.0°$ and $\Phi = 92.7°$. Previously calculated geometries of ground state of $HSiCN^-$ and $HSiNC^-$ were quite close to ours.

It is now generally accepted that neutral molecules with dipole moments $\mu \geq 2.5$ D can form dipole-bound negative ions [36–48]. Owing to its large dipole moment of 3.2 and 3.3 D, HSiCN and HSiNC readily attach an 'excess' electron in a dipole-bound state, and since its unsaturated π-system virtually guarantees the existence of a low-lying valence anion state X^2A''. In such ions the electron is weakly bound by the dipole potential of the neutral molecule and is localized near the positive end of the dipole in a diffuse orbital. There are dipole-bound $^2A'$ negative ion states of $HSiCN^-$ and $HSiNC^-$ with an AEA value of 3.11×10^{-4} and -0.74 eV, respectively. Table 7 gives the Mulliken population analysis for the X^2A'', $^2A'$, $^4A''$, and $^4A'$ states of HSiCN, HSiNC anions. From the Mulliken population analysis, we can see that electron attachment to the neutral give rise to the dipole-bound $^2A'$, $^4A''$, and $^4A'$ anion excited states of $HSiCN^-$, $HSiNC^-$, and the extra electron in the dipole-bound states $^2A'$ and $^4A'$ of HSiCN and HSiNC resides mainly beyond H atom. While for the $^4A'$ of HSiCN and of HSiNC, the excess electron resides on the Si atom.

3 Conclusion

We have investigated the ground-state and low-lying excited states of HSiCN and HSiNC using the CASSCF and CASPT2 methods. The cyanosilylene and isocyanosilylene both have the singlet ground state. The CN and NC group substituents enhance the singlet–triplet gap of SiH_2. The vertical excitation energies of singlet and triplet states of HSiCN and HSiNC show that the lowest excitation energies in HSiCN are lower than those in HSiNC. In dipole allowed excitation, the vertical transition energy of $X^1A' \rightarrow {}^1A''$ is the lowest, and $X^1A' \rightarrow 3^1A'$ transition is the most intensive transition for HSiCN; $X^1A' \rightarrow {}^1A''$ is the lowest and most intensive transition for HSiNC. The first vertical and adiabatic ionization energies of HSiCN are

higher than that of HSiNC. Neither cyanosilylene (HSiCN) nor isocyanosilylene (HSiNC) possesses valence-bound excited negative ion states. All excited negative ion states can be characterized as dipole-bound states.

References

1. Duley WW, Williams DA (1984) Interstellar chemistry. Academic Press, London
2. Cernicharo J, Gottlieb CA, Guelin M, Thaddeus P, Vrtilek JM (1989) Astrophys J 341:L25. doi:10.1086/185449
3. Guelin M, Muller S, Cernicharo J, Apponi AJ, McCarthy MC, Gottlieb CA, Thaddeus P (2000) Astron Astrophys 363:L9
4. Guelin M, Muller S, Cernicharo J, McCarthy MC, Thaddeus P (2004) Astron Astrophys 426:L49. doi:10.1051/0004-6361:200400074
5. Apponi AJ, McCarthy MC, Gottlieb CA, Thaddeus P (1999) Astrophys J 516:L103. doi:10.1086/311998
6. Wang Q, Ding YH, Sun CC (2006) Chem Phys 323:413. doi:10.1016/j.chemphys.2005.09.043
7. Stanton JF, Dudek J, Theule P, Gupta H, McCarthy MC, Thaddeus P (2005) J Chem Phys 122
8. Flores JR, Perez-Juste I, Carballeira L (2005) Chem Phys 313:1. doi:10.1016/j.chemphys.2004.12.009
9. Liu HL, Huang XR, Chen GH, Ding YH, Sun CC (2004) J Phys Chem A 108:6919. doi:10.1021/jp0484074
10. McCarthy MC, Gottlieb CA, Thaddeus P (2003) Mol Phys 101:697. doi:10.1080/0026897021000035197
11. McCarthy MC, Thaddeus P (2002) J Mol Spectrosc 211:228. doi:10.1006/jmsp.2001.8467
12. Andersson K et al (2005) MOLCAS. Version 6.2. University of Lund, Sweden
13. Srinivas R, Vivekananda S, Schroder D, Schwarz H (2000) Chem Phys Lett 316:243. doi:10.1016/S0009-2614(99)01253-1
14. Apponi AJ, McCarthy MC, Gottlieb CA, Thaddeus P (2000) Astrophys J 536:L55. doi:10.1086/312719
15. Bailleux S, Bogey M, Breidung J, Burger H, Fajgar R, Liu YY, Pola J, Senzlober M, Thiel W (1996) Angew Chem Int Ed Engl 35:2513. doi:10.1002/anie.199625131
16. Sanz ME, McCarthy MC, Thaddeus P (2002) Astrophys J 577:L71. doi:10.1086/344083
17. Dover MR, Evans CJ (2007) J Phys Chem A 111:13148. doi:10.1021/jp076289p
18. Kalcher J (2005) J Phys Chem A 109:11437. doi:10.1021/jp0534840
19. Wei ZZ, Li BT, Zhang HX, Sun CC, Han KL (2006) J Comput Chem 28:467. doi:10.1002/jcc.20538
20. Li BT, Wei ZZ, Zhang HX, Sun CC (2006) J Phys Chem A 110:10643. doi:10.1021/jp063003s
21. Hou CY, Zhang HX, Sun CC (2006) J Phys Chem A 110:10260. doi:10.1021/jp060528b
22. Hou CY, Zheng QC, Zhao ZX, Zhang HX, Sun CC (2007) J Phys Chem A 111:12037. doi:10.1021/jp072017a
23. Zhao ZX, Zhang HX, Sun CC (2008) J Phys Chem A 112:12125. doi:10.1021/jp8070663
24. Roos BO (1987) In Adv. In: Lawley KP (ed) Ab Initio Methods in Quantum Chemistry-II. Wiley, Chichester, p 399
25. Bernhardsson A, Lindh R, Olsen J (1999) And Fülscher. M Mol Phys 99:103
26. Serrano-Andres L, Merchan M, Nebot-Gil I, Lindh R, Roos BO (1993) J Chem Phys 98:3151. doi:10.1063/1.465071
27. Dunning T (1989) J Chem Phys 90:1007. doi:10.1063/1.456153
28. Woon DE, Dunning T (1993) J Chem Phys 98:1358. doi:10.1063/1.464303
29. Andersson K et al (2004) MOLCAS, version 6.0. University of Lund, Sweden
30. Yamada C, Kanamori H, Hirota E, NIshiwaki N, Itabashi N, Kato K, Goto T (1989) J Chem Phys 91:4582. doi:10.1063/1.456746
31. Grev RS, Schaefer HF, Gaspar PP (1991) J Am Chem Soc 113:5638. doi:10.1021/ja00015a017
32. Apeloig Y, Pauncz R, Karni M, West R, Steiner W, Chapman D (2003) Oragnometallics 22:3250. doi:10.1021/om0302591
33. Muramoo Y, Ishikawa H, Mikami NJ (2005) Chem Phys 122:154302
34. Guerout R, Bunker PRJ (2005) Chem Phys 123:244312
35. Linstrom PJ, Mallard WG (eds) (2005) Chemistry NIST WebBook. http://webbook.nist.gov/chemistry/
36. Lykke KR, Neumark DM, Anderson T, Trapa VJ, Lineberger WC (1987) J Chem Phys 87:6842. doi:10.1063/1.453379
37. Marks J, Brauman JI, Mead RD, Lykke KR, Lineberger WC (1988) J Chem Phys 88:785. doi:10.1063/1.454424
38. Brinkman EA, Berger S, Marks J, Brauman JIJ (1993) Chem Phys 99:7586
39. Desfrançois C, Abdoul-Carime H, Adjouri C, Khelifa N, Schermann J-P (1994) Europhys Lett 26:25. doi:10.1209/0295-5075/26/1/005
40. Popple RA, Finch CD, Dunning FB (1995) Chem Phys Lett 234:172. doi:10.1016/0009-2614(95)00043-4
41. Abdoul-Carime H, Desfrançois C (1998) Eur Phys J D 2:149
42. Lecomte F, Carles S, Desfrançois CJ (2000) Chem Phys 113:10973
43. Suess L, Liu Y, Parthasarathy R, Dunning FB (2003) Chem Phys Lett 376:376. doi:10.1016/S0009-2614(03)00990-4
44. Hammer NI, Jordan KD, Desfrançois C, Compton RNJ (2003) Chem Phys 119:3650
45. Suess L, Liu Y, Parthasarathy P, Dunning FBJ (2004) Chem Phys 121:7162
46. Clary DCJ (1988) Phys Chem 92:3173. doi:10.1021/j100322a028
47. Simons JJ (1989) Chem Phys 91:6858
48. Giri PR, Gupta KS, Meijanac S, Samsarov A (2008) Phys Lett A 372:2967. doi:10.1016/j.physleta.2008.01.008